forests

MDPI

Article

Comparison of Wood Porosity Profiles Obtained by Two Measurement Methods: The Tracheidogram Method and Pixel-Contrast Densitometry

Timofey A. Khudykh [1,*], Liliana V. Belokopytova [1,2], Denis G. Portnyagin [2], Vlad A. Vasilishin [2,3], Dina F. Zhirnova [1,2], Nariman B. Mapitov [4], Elena A. Babushkina [1,2] and Eugene A. Vaganov [1,5]

[1] Institute of Ecology and Geography, Siberian Federal University, Krasnoyarsk 660041, Russia; white_lili@mail.ru (L.V.B.); dina-zhirnova@mail.ru (D.F.Z.); babushkina70@mail.ru (E.A.B.); eavaganov@hotmail.com (E.A.V.)
[2] Khakass Technical Institute, Siberian Federal University, Abakan 655017, Russia; my4455@yandex.ru (D.G.P.); vasilishin.vladislav@hotmail.com (V.A.V.)
[3] Institute of Forest Technologies, Reshetnev Siberian State University of Science and Technology, Krasnoyarsk 660037, Russia
[4] Department of Biology and Ecology, Toraighyrov University, 64 Lomov Street, Pavlodar 140008, Kazakhstan; mapitov@mail.ru
[5] V.N. Sukachev Institute of Forest, Federal Research Center "Krasnoyarsk Science Center of the Siberian Branch of the Russian Academy of Sciences" (FRC KSC SB RAS), Krasnoyarsk 660036, Russia
* Correspondence: khudykta@gmail.com; Tel.: +7-(906)-972-1630

Abstract

Pixel-contrast (PiC) densitometry is a new automated method for obtaining high-resolution intra-ring wood porosity profiles, but its use in dendroclimatology requires validation against established approaches. We compared porosity profiles of 836 tree rings of *Pinus sylvestris* L. and *Picea obovata* Ledeb. (2000–2020) from experimental plantations of different stand densities in the southern taiga of Krasnoyarsk Krai, Russia. Anatomical porosity (P_{anat}) was calculated from tracheidograms using a simplified geometric cell model, and PiC porosity (P_{pic}) from wood cross-section images segmented by a U-Net neural network. Agreement between these estimates was assessed using linear regression, mean absolute percentage error and root mean square error for the total ring, earlywood and latewood. The relationship between the estimates for whole rings was strong (R^2 = 0.79–0.93) and stable across ring widths, but weak in earlywood (R^2 = 0.24–0.46). However, a substantial part of this whole-ring agreement reflects the shared decrease in porosity from earlywood to latewood; after removing the species mean profile, R^2 was 0.57 in spruce and 0.42 in pine. P_{anat} systematically exceeded P_{pic} in all ring zones (median differences 0.04–0.08 at an assumed tangential cell diameter of 30 μm), more so in pine, where the excess increased in latewood. The discrepancies are most likely due to the selection of large, regularly shaped tracheids for tracheidogram measurements and the assumption of equal radial and tangential cell wall thicknesses. Both estimates reproduce the general course of porosity within the ring, but their equivalence for dendroclimatic analysis requires separate testing, whereas for comparisons of absolute values P_{pic} should be regarded as more representative of the bulk cross-sectional porosity, as it integrates all anatomical elements across the scanned area.

Keywords: dendroecology; wood porosity; digital wood anatomy; image analysis; conifers; tracheidogram; pixel-contrast densitometry; *Pinus sylvestris*; *Picea obovata*

Academic Editors: Álvaro Rubio-Cuadrado, Marco Fioravanti and Tomasz Jelonek

Received: 19 October 2026
Revised: 23 November 2026
Accepted: 24 November 2026
Published: 25 November 2026

Copyright: © 2026 by the authors. Licensee MDPI, Basel, Switzerland. This article is an open access article distributed under the terms and conditions of the Creative Commons Attribution (CC BY) license.

1. Introduction

Digital methods, including ROXAS, have advanced quantitative wood anatomy [1,2]. Anatomical measurements have been used to study cambial activity and environmental responses in conifers [3,4]. They have also been explored as dendroclimatic proxies and as a basis for studying sub-seasonal responses [5,6]. The development of digital wood anatomy has stimulated several related research directions: the formulation of new hypotheses on the control of tree-ring structure [7,8], a more detailed consideration of the role of hormones and gene expression in xylogenesis [9–11]. Studies have examined tree growth phenology and the timing and biological basis of cambial activity [12–14]. Other studies have examined how climate influences xylem morphogenesis and cambial activity during the growing season [15,16]. Models have also been used to investigate how climatic factors affect the production, enlargement, and maturation of xylem cells [17]. Although conifer wood is relatively homogeneous because tracheids dominate its structure, the transition from earlywood to latewood introduces a marked within-ring contrast as lumina narrow and cell walls thicken [18–20].

Pixel-contrast densitometry (PiC densitometry) is a promising direction in digital wood anatomy [21]. Its applicability extends beyond conifers to angiosperm woody species with ring-porous or diffuse-porous wood [22]. In conifers, PiC densitometry is technically similar to measurements performed using the ROXAS software because it can be applied to stained thin cross-sections of tree rings and to well-prepared, finely polished wood cores or discs [1]. A specialized computer program for PiC densitometry has been developed and continues to be improved at the dendroecological laboratory of the Khakass Technical Institute, Siberian Federal University. It is available to researchers and to undergraduate and graduate students [22]. Silkin et al. [21] compared the results of PiC densitometry with X-ray densitometry data from Scots pine samples; the chronologies of most parameters were highly correlated, whereas the agreement was lower for earlywood mean density and minimum density. One of the outputs of PiC densitometry is the profile of wood porosity (the proportion of cell lumina in the cross-sectional area) within individual tree rings at high spatial resolution; later, PiC densitometry was used to obtain wood porosity profiles and to compare the climate responses of this variable in Scots pine and aspen [22].

The tracheidogram method, based on measuring the radial cell diameter and cell wall thickness along radial files of tracheids, was developed for analyzing the structure of conifer tree rings [23] and is widely used to measure anatomical traits along radial tracheid files [24,25]. Such measurements have also been applied to studies of tree-ring structure and its relationship with climate [7,15]. It also makes it possible to calculate a tree-ring porosity profile from anatomical measurements, albeit with lower resolution and some error.

Accurate estimation of wood porosity is important because this characteristic underlies many structural and functional properties of wood. Since the density of cell-wall material is nearly constant (about 1.5 g/cm^3 [26]), wood density and its variation within a tree ring are determined by the proportion of cell-wall material, i.e., by porosity, which in turn depends on tracheid lumen size and cell wall thickness. Changes in wall-matter accumulation have been documented in spruce [27], and within-ring wood density has been linked to tracheid anatomy in Douglas fir [28]. The anatomical basis of conifer wood-density variation has also been discussed more broadly [29] and examined in a biophysical model of *Pinus pinaster* exposed to seasonal drought [30].

Wood density is a key predictor of mechanical properties [31], and the ratio of cell wall thickness to lumen size determines tracheid stiffness and the resistance of xylem to implosion [32,33]. Models of conifer hydraulic function account for tracheid and pit structure [34] and allow conductivity to be estimated within and between annual rings from

https://doi.org/10.3390/f17121430

anatomical data [35]. Reviews of Pinaceae and conifer xylem place these relationships in a broader functional context [36,37]. Finally, porosity and density profiles within a ring reflect the seasonal dynamics of cambial activity and growth conditions and therefore serve as a data source for dendroclimatic analysis and reconstructions [5,22,38]. Thus, systematic differences between porosity measurement methods may affect both absolute values and the comparability of data across studies, which makes a quantitative assessment of the agreement between these methods necessary. However, porosity profiles obtained by PiC densitometry have not yet been systematically compared with porosity calculated from tracheidogram data in conifers. This study aims to fill this gap by comparing the porosity profiles obtained by the two methods for 836 tree rings of two conifer species that differ in ring width and number of cells. A comparison of the tracheidogram and pixel-contrast methods is of interest for several reasons. First, pixel-contrast densitometry is a relatively new automated method, and its broad application in dendroclimatic and dendroecological studies requires validation against the well-established tracheidogram method. Second, the calculation of porosity from tracheidograms relies on simplified formulae for total cell and cell wall areas, which inevitably introduces discrepancies between calculated values and the resulting wood porosity. Third, the methods differ fundamentally in the set of wood components being measured: tracheidogram measurements are made only along visually selected radial files of large tracheids of relatively regular shape, whereas PiC densitometry includes all cells of the scan in the porosity calculation, including smaller tracheids, ray parenchyma and resin ducts. This difference in the measured object can potentially lead to a systematic discrepancy between the porosity profiles obtained by the two methods.

The aim of this study was to compare detailed measurements (profiles) of tree-ring porosity of conifers obtained by pixel-contrast densitometry and by the tracheidogram method, and to assess to what extent the discrepancies between them are explained by differences in the set of measured anatomical wood components. To achieve this aim, the following objectives were addressed: (1) to compare the porosity profiles calculated by the two methods for tree rings differing in width and cell number; (2) to assess the consistency between the methods in different functional anatomical zones of the tree ring (earlywood and latewood); and (3) to analyze the possible causes of the revealed discrepancies on the basis of the differences in the measurement principles of the two methods.

Two coniferous species were selected for the comparative analysis, Scots pine (*Pinus sylvestris* L.) and Siberian spruce (*Picea obovata* Ledeb.), whose tracheidograms had been obtained and published previously [39].

2. Materials and Methods

2.1. Study Area and Obtaining of Wood Structure Images

Wood samples were collected in experimental conifer plantation plots of different stand densities in the Bolshemurtinsky District of Krasnoyarsk Krai, in the zone of typical southern taiga. The plantation was established in 1982 by the staff of the Institute of Forest, Siberian Branch of the USSR Academy of Sciences (Krasnoyarsk), near the village of Talovka (57°12′18″ N, 93°08′36″ E, 240 m a.s.l.). The climate of the region is temperate continental. Detailed descriptions of the study area and the experimental plantation are given in previous publications [40,41].

For the analysis of wood structure, six plots were selected for each species, with stand densities ranging from 0.75 to 96 thousand trees per hectare at planting (0.4–18 thousand trees per hectare at the 2015 inventory), and five trees per site were sampled. The measurement period was restricted to 2000–2020 (age of 20 years and older) to avoid juvenile wood, which in the study area is characterized by the frequent formation of frost rings with irregular cell structure [39].

https://doi.org/10.3390/f17121430

In both approaches to wood porosity estimation, wood cross-sections 18–20 μm thick were used; they were cut from cores on a MICROM HM430 rotary microtome (Thermo Fisher Scientific, Waltham, MA, USA), stained with a 1% aqueous solution of safranin and Astra blue (1:1; lignified wood matter stains dark red, non-lignified tissues stain blue) and fixed in glycerol. The same digital images of sections in this glycerol-saturated state were used for both the tracheidogram measurements and PiC densitometry. Images of the sections were obtained at 400× magnification using a BX43 light microscope (Olympus, Tokyo, Japan) and a ProgRes Gryphax Subra digital camera (Jenoptik, Jena, Germany). The imaging parameters were standardized: exposure 1/60 s, ISO 200, white balance 5200 K. The image scale was calibrated for this microscope–camera system and equaled 0.42604 μm per pixel; the same scale was used for both methods.

For the comparative analysis of the two porosity estimation methods in this study, from the full bank of anatomical measurements (more than 1200 tree rings: 2 species × 6 sites × 5 trees × 21 years) we selected the rings that had no structural anomalies, such as irregular tracheid files [18], and whose images were large enough in the tangential direction for five replicate measurements of PiC densitometric porosity (1800 pixels).

2.2. Anatomical Measurements and Calculation of Anatomical Wood Porosity

Tracheidograms were measured using the Lineyka software (version 2.03; Silkin, Krasnoyarsk, Russia [24]) according to the classical procedure [23–25] (Figure 1). In each ring, the radial lumen diameter (L_r) and the double cell wall thickness (2CWT) were measured sequentially along five radial files of tracheids, from the first earlywood cell to the last latewood cell, with an accuracy of 0.01 μm. The radial diameter of each tracheid was then derived as $D_r = L_r + 2CWT$ [24]. The resulting tracheidograms were standardized to the mean number of cells per ring (by stretching or compressing the file length; [23]) and averaged over the five radial files.

Table 1 presents quantitative data on the variability of cell number in pine and spruce tree rings. It is easy to see that the stand density gradient, which remained stable despite self-thinning, provided a high diversity of annual wood increment, expressed as the number of tracheids per radial file (produced by a single initial), even with the period of anatomical measurements restricted to 2000–2020. According to these data, the ratio of the mean cell number between stands of different density reaches 3.4 for pine tree rings and up to 4.2 for spruce tree rings. Across the whole sample, the number of cells varies from 5–6 to almost 200. This makes it possible to obtain more representative results when comparing pixel-contrast densitometry and the tracheidogram method.

Table 1. Data on the studied tree rings of *Picea obovata* and *Pinus sylvestris*: number of selected rings in different ranges of cell number per radial file and on sites with different stand density.

Species	Stand Density, Thousand Trees/ha		Number of Studied Tree Rings by Ranges of Cell Number per Radial File					Variability of Cell Number per Radial File: Mean (Min–Max)
	Planting in 1982	Inventory in 2015	5–25	26–50	51–75	76–200	Total	
Picea obovata	0.75	0.38	0	2	8	34	44	125 (31–198)
	2.00	1.06	5	27	10	26	68	74 (19–172)
	6.00	2.15	11	26	12	16	65	56 (7–163)
	12.00	4.26	28	18	3	3	52	30 (6–100)
	32.00	6.19	27	49	6	0	82	33 (10–66)
	96.00	18.05	27	36	22	0	85	37 (11–72)
	all		98	158	61	79	396	55 (6–198)
Pinus sylvestris	0.75	0.43	0	6	25	44	75	98 (39–191)
	2.00	1.06	0	20	39	25	84	68 (27–143)

https://doi.org/10.3390/f17121430

4.00	2.30	21	45	28	0	94	40 (11–71)
12.00	6.27	3	64	17	0	84	42 (13–67)
32.00	7.18	4	35	19	3	61	48 (9–92)
96.00	8.37	20	16	6	0	42	29 (5–61)
all		48	186	134	72	440	56 (5–191)

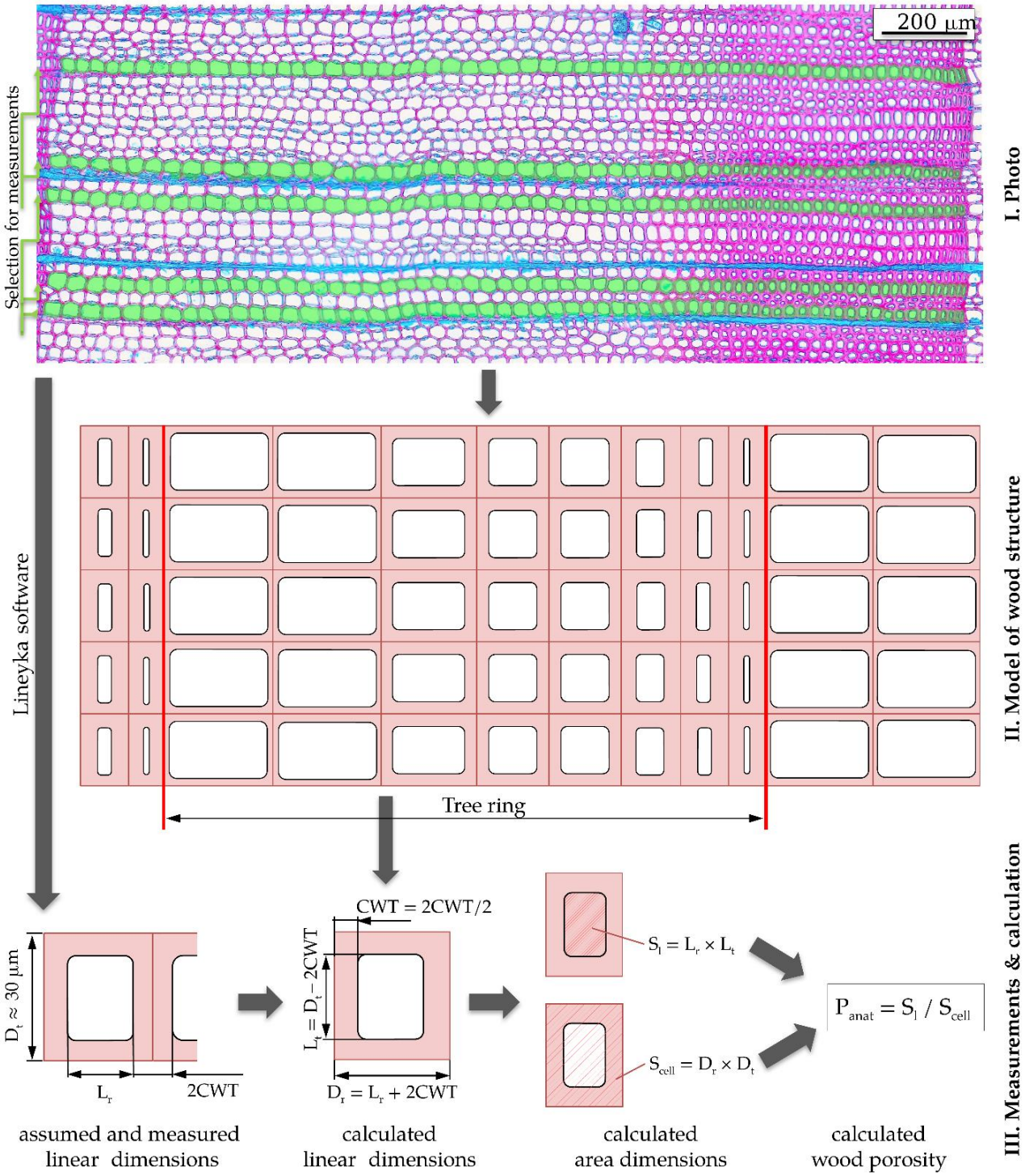


Figure 1. Three-step procedure for the anatomical estimation of wood porosity: (I) fragment of a tree-ring image with the radial cell files selected for anatomical measurements highlighted; (II) scheme of the simplified geometric model of the wood cell structure with rectangular cells and uniform cell wall deposition in all directions; (III) measurements and calculation of the anatomical porosity of a tracheid (P_{anat}). Shown are the empirically assumed mean tangential cell diameter (D_t);

the radially measured lumen diameter (L_r) and double cell wall thickness (2CWT); and the values calculated from them: radial cell diameter (D_r), cell wall thickness (CWT), tangential lumen diameter (L_t), lumen area (S_l), cell area (S_{cell}) and anatomical porosity of the given cell (P_{anat}).

Several assumptions were made in calculating porosity from tracheidogram measurements:

1. The cross-sectional shape of the cell (tracheid) was conventionally assumed to be rectangular.
2. The thickness of the tangential walls was assumed to be equal to the measured thickness of the radial walls. This is an intentional simplification, and its validity decreases in latewood.
3. The tangential cell diameter was assumed to be 30 μm, which corresponds to the mean tangential tracheid diameter of boreal conifers measured with a similar sampling procedure. For comparison, [27] reported mean tangential tracheid diameters of 24.9–28.2 μm for Siberian spruce in the mountains of southern Siberia, depending on elevation. For Scots pine, the mean tangential tracheid diameter reported by [42] is 29.8 μm (30.3 μm in earlywood and 29.4 μm in latewood), and for Norway spruce, a close relative of Siberian spruce, 30.8 μm (31.2 and 30.3 μm, respectively) [43]. Thus, the assumed value is close to the known means for both species and almost independent of the ring zone. In this study, "radial wall thickness" and "tangential wall thickness" refer to wall thickness measured in the radial and tangential directions, respectively. This measurement-based terminology is used throughout the manuscript and is illustrated in Figure 1.

Knowing the radial lumen diameter and the double cell wall thickness, the other linear dimensions of the cell and its elements can be calculated, followed by the lumen and total cell areas using the formulae given in Figure 1. Finally, the anatomical porosity of a cell is defined as the ratio of the lumen area to the total cell area.

Note that our assumptions and simplifications are similar to those used in previously published studies by Russian and international authors modeling tracheid structure and function (e.g., [24,34,44]).

To assess the possible effect of cell-wall anisotropy, we defined the ratio of tangential-wall thickness (CWTt) to the measured radial-wall thickness (CWT) as $k_w = CWT_t/CWT$. For latewood cells, P_{anat} was recalculated assuming that the thickness of the tangential wall is equal to:

$$CWT_t = k_w \times CWT \quad (1)$$

where the coefficient k_w was varied from 1.0 to 1.5 in steps of 0.1 ($k_w = 1$ was assumed for earlywood). For all tree rings of each species pooled (at $D_t = 30$ μm), the coefficient of determination (R^2), the slope of the regression line, the root mean square error (RMSE), and the median difference $P_{anat} - P_{pic}$ were recalculated.

2.3. PiC Densitometric Estimation of Wood Porosity

Porosity analysis by PiC densitometry was performed using original specialized software (available at: https://github.com/Timofey00/OpenPiCDens; accessed on 19 October 2026) based on machine learning algorithms for the automatic segmentation of anatomical images [22]. The original RGB images of wood cross-sections (Figure 1) were converted to grayscale and subjected to median smoothing to remove noise while preserving cell wall boundaries [45]. Cell walls and lumina were segmented automatically using a neural network with the U-Net architecture implemented in the segmentation-models-pytorch library [46]. The image binarization procedure is described in more detail in Khudykh et al. [22].

Porosity profiles were constructed using a virtual scanning sensor 1000 pixels (~426 μm) wide in the tangential direction and 1 pixel in the radial direction. For replicate measurements of each ring, a series of five overlapping images with a step of 200 pixels (~85 μm) in the tangential direction was obtained, each covering the full radial extent of the ring from the boundary with the preceding ring to the boundary with the following one. The ratio of lumen (image pixels not occupied by cell walls) to the total area of the scanning probe was then measured automatically. That is, for each sensor position, porosity P_{pic} was calculated as the ratio of the number of white pixels, which correspond to the lumen pixels on the image, to the total number of pixels in the scanned area. Resin ducts were removed from the profile at this stage: continuous runs of lumen pixels longer than 150 pixels (~64 μm) along the scanning line were removed from the line and excluded from the calculation (gap_value = 150 in OpenPiCDens). The final porosity profile was obtained by averaging the values of all five overlapping measurements, which ensured the statistical robustness of the results to minor anatomical fluctuations.

Next, to compare the porosity profiles obtained by PiC densitometry and by the tracheidogram method, each tree ring was divided into narrow bands proportional to the radial diameters D_r in the averaged standardized tracheidogram, and PiC densitometric porosity was averaged within each band (cf. [3,15]). Thus, for each tree ring, the same number of porosity data points was obtained for both methods, with one-to-one correspondence between them.

The consistency between the methods was assessed using the coefficient of determination (R^2) and the coefficients of linear regression between the P_{anat} and P_{pic} profiles. A classical linear function with an intercept was used ($P_{anat} = a\,P_{pic} + b$, where a is the slope and b is the intercept); thus, the slope characterizes the steepness of the relationship between the profiles rather than being a direct measure of the ratio between the porosity estimates obtained by the different methods. To estimate the magnitude and direction of the discrepancy, we used the mean absolute percentage error:

$$MAPE = 100\% \cdot \sum \left|P_{anat} - P_{pic}\right| / \left(n \cdot P_{pic}\right) \quad (2)$$

and the root mean square error:

$$RMSE = \sqrt{\sum \left(P_{anat} - P_{pic}\right)^2 / n} \quad (3)$$

as well as the difference between the porosity estimates:

$$Diff\left(P_{anat}, P_{pic}\right) = P_{anat} - P_{pic} \quad (4)$$

MAPE and *RMSE* are commonly used to assess the accuracy of model predictions [47,48]. To assess the agreement between the methods in different functional zones of the tree ring, the profiles were additionally divided into earlywood (EW) and latewood (LW); the EW/LW boundary was defined as the point of the profile corresponding to the median P_{pic} value within the ring, taking into consideration continuity of zones: latewood was taken as the continuous run of cells from the end of the ring in which P_{pic} did not exceed this median. This boundary corresponds, on average, to $CWT/D \approx 0.10$ at the first latewood cell in both species, which is close to the species-specific thresholds of the ratio of cell wall thickness to cell diameter ($k = CWT/D = 0.105$ for *Picea obovata* and 0.110 for *Pinus sylvestris*) proposed for distinguishing earlywood and latewood tracheids [49]. To test the dependence of the results on this choice, the comparison was repeated with three alternative boundaries: the median P_{anat} in the ring (determined by the same procedure, counted from the end of the ring), the threshold $CWT/D \geq k$ [49], and the Mork criterion in the form $4 \cdot CWT \geq L_r$, i.e., $CWT/D \geq 1/6$ [50], where L_r is the radial lumen diameter. To further assess the agreement between the methods, we examined to what extent the relationship

between them is determined by the common decreasing trend of porosity profiles from earlywood to latewood. For this purpose, the mean profile of each species (the mean values of P_{pic} and P_{anat} as functions of the relative position within the tree ring, divided into 40 equal intervals) was subtracted from the values of both estimates. The coefficient of determination R^2 was then recalculated for the resulting residuals. The discrepancy between the methods at each position was characterized by the standard deviation of the pair of values (P_{pic}, P_{anat}) of each cell, i.e., $|P_{anat} - P_{pic}|/\sqrt{2}$, averaged over the intervals of relative position and compared with the standard deviation of P_{pic} among rings in the same interval.

3. Results

As an example, let us consider one tree ring of average width for spruce and pine each (Figure 2). In pine, the PiC estimate was lower than the anatomical estimate throughout the ring. The mean difference (anatomical minus PiC) was 0.07 in earlywood and 0.12 in latewood, reaching 0.22–0.24 in the final two cells. In spruce, the profiles were similar through most of the ring, but the PiC estimate was lower than the anatomical estimate by 0.08–0.12 in the final seven latewood cells.

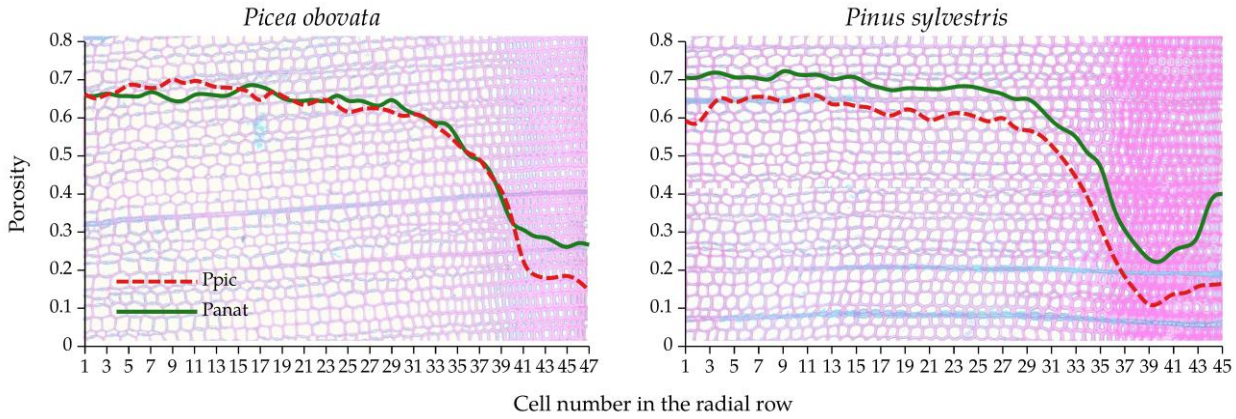


Figure 2. Typical porosity profiles obtained by PiC densitometry and by the tracheidogram method for *Picea obovata* and *Pinus sylvestris*, illustrated by tree rings with an average cell number sampled on the site with the sparsest planting. P_{pic}, red dashed line; P_{anat}, green solid line. The corresponding images of wood cross-sections are shown in the background.

The comparison of porosity values calculated by PiC densitometry and from tracheidograms for rings of different width (and different cell number per radial file, since these variables are related by practically direct proportionality [39]) revealed common patterns (Figure 3). Overall, both species behaved similarly: in spruce, as in pine, P_{anat} exceeds P_{pic} in all groups and in both ring zones, i.e., in both earlywood and latewood. Except for the widest rings, the difference between anatomical and PiC densitometric porosity is larger in pine than in spruce. For both species, the entire interquartile range of this difference is positive, and its medians lie within 0.04–0.05 for spruce and 0.04–0.08 for pine.

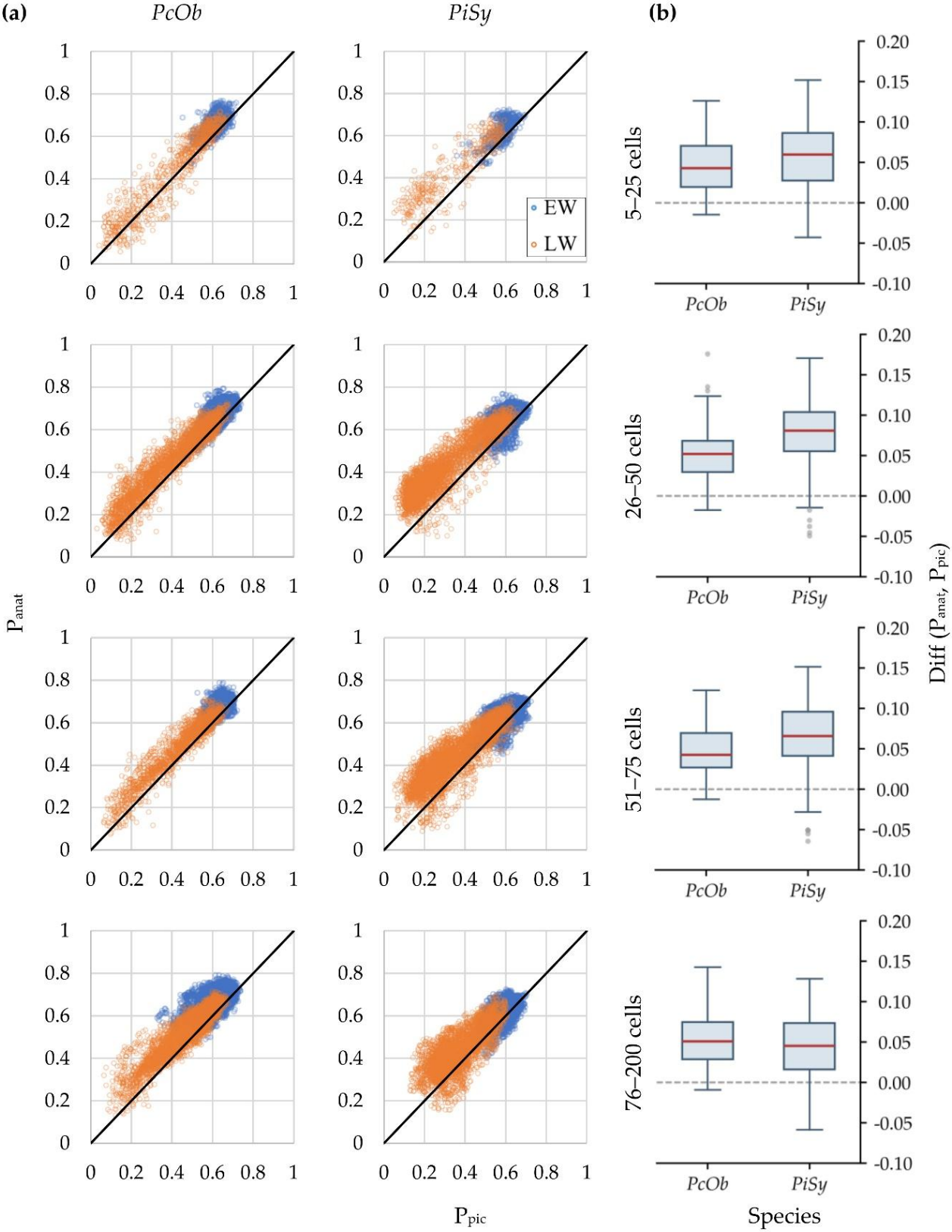


Figure 3. Comparison of porosity values obtained by the two methods for tree rings of spruce (*PcOb*) and pine (*PiSy*) classified by the number of cells per radial file: (**a**) scatter plots with the earlywood (EW, blue) and latewood (LW, orange) zones highlighted in color; the diagonal represents the 1:1 ratio of porosity values; (**b**) main characteristics of the distribution of the difference between the two porosity estimates ($P_{anat} - P_{pic}$): 25th and 75th percentiles (box), median (horizontal line), extreme values within 1.5 interquartile ranges (whiskers), and outliers (points beyond the whiskers).

https://doi.org/10.3390/f17121430

The analysis of the linear functions $P_{anat}(P_{pic})$ revealed new patterns (Table 2). When the tree ring was considered as a whole, R^2 was high in both species regardless of ring width (from 0.79 to 0.93). The slope ranged from 0.8 to 1.0 in spruce. In pine, the slope was substantially below 1.0 in all groups (about 0.8). The stable excess of P_{anat} over P_{pic} at such slope values is due to the positive regression intercept (0.04–0.16 in spruce and 0.15–0.19 in pine), i.e., to a more pronounced difference in the latewood zone. It is also latewood, with its wide range of porosity variability, that provides the high coefficient of determination in the model for the total ring, since in earlywood this parameter does not exceed 0.5 in either species. In absolute terms, *RMSE* in spruce is relatively stable (0.06–0.08) for all ring zones and for rings of different width, whereas in pine this parameter is consistently higher in latewood (0.10–0.13) than in earlywood (0.05–0.07). However, in terms of the relative (percentage) difference, *MAPE* in latewood is several times higher in both species. Thus, the difference between the porosity estimates is more stable in absolute than in relative terms.

Table 2. Parameters of the linear regression relationship between the porosity estimates $P_{anat}(P_{pic})$ for tree rings grouped by the number of cells per radial file. R^2, coefficient of determination; *a*, slope of the regression line; *b*, intercept; *MAPE*, mean absolute percentage error; *RMSE*, root mean square error.

Cell Number	Tree-Ring Zone	*Picea obovata*					*Pinus sylvestris*				
		R^2	*a*	*b*	*MAPE*, %	*RMSE*	R^2	*a*	*b*	*MAPE*, %	*RMSE*
5–25	Total ring	0.91	1.01	0.04	14.92	0.07	0.86	0.79	0.16	27.18	0.09
	EW	0.28	0.55	0.33	9.02	0.07	0.43	0.75	0.18	8.76	0.06
	LW	0.89	0.99	0.04	21.59	0.07	0.81	0.80	0.16	47.31	0.12
26–50	Total ring	0.93	0.91	0.10	15.64	0.07	0.89	0.77	0.19	30.18	0.10
	EW	0.46	0.73	0.21	7.54	0.06	0.24	0.51	0.35	9.67	0.07
	LW	0.90	0.90	0.10	24.54	0.08	0.81	0.78	0.18	53.56	0.13
51–75	Total ring	0.92	0.91	0.10	12.05	0.06	0.85	0.76	0.18	22.74	0.09
	EW	0.25	0.52	0.35	7.27	0.06	0.33	0.56	0.30	8.54	0.06
	LW	0.90	0.90	0.10	17.89	0.07	0.74	0.76	0.17	39.84	0.12
76–200	Total ring	0.81	0.83	0.16	12.96	0.08	0.79	0.78	0.15	14.61	0.07
	EW	0.35	0.50	0.36	10.26	0.07	0.26	0.53	0.31	6.67	0.05
	LW	0.83	0.80	0.15	17.63	0.08	0.58	0.73	0.17	24.86	0.10
All	Total ring	0.89	0.90	0.11	13.70	0.07	0.84	0.77	0.17	22.39	0.09
	EW	0.35	0.54	0.34	9.00	0.07	0.29	0.57	0.30	8.23	0.06
	LW	0.88	0.89	0.10	20.20	0.08	0.72	0.75	0.18	39.49	0.11

Pooling the comparison results for all groups of tree rings, we finally obtained the plots for the two studied species (Figure 4). A systematic excess of P_{anat} over P_{pic} is observed along the entire tree ring. It should be noted, however, that in spruce the ratio between them is more stable across the functional zones of the ring, whereas in pine the excess increases in latewood, as indicated both by the lower slope of the regression model (Table 2) and by the values of the difference between P_{anat} and P_{pic} (in Figure 4b, the median difference in pine latewood is almost twice that in earlywood, while in spruce the ranges of the difference are stable throughout the ring). *MAPE* was also considerably higher for pine than for spruce, whereas the difference in *RMSE* was minor, although in pine this parameter varies more among tree-ring zones. Overall, the patterns revealed when rings of different width were considered separately are, as expected, also observed for the whole sample.

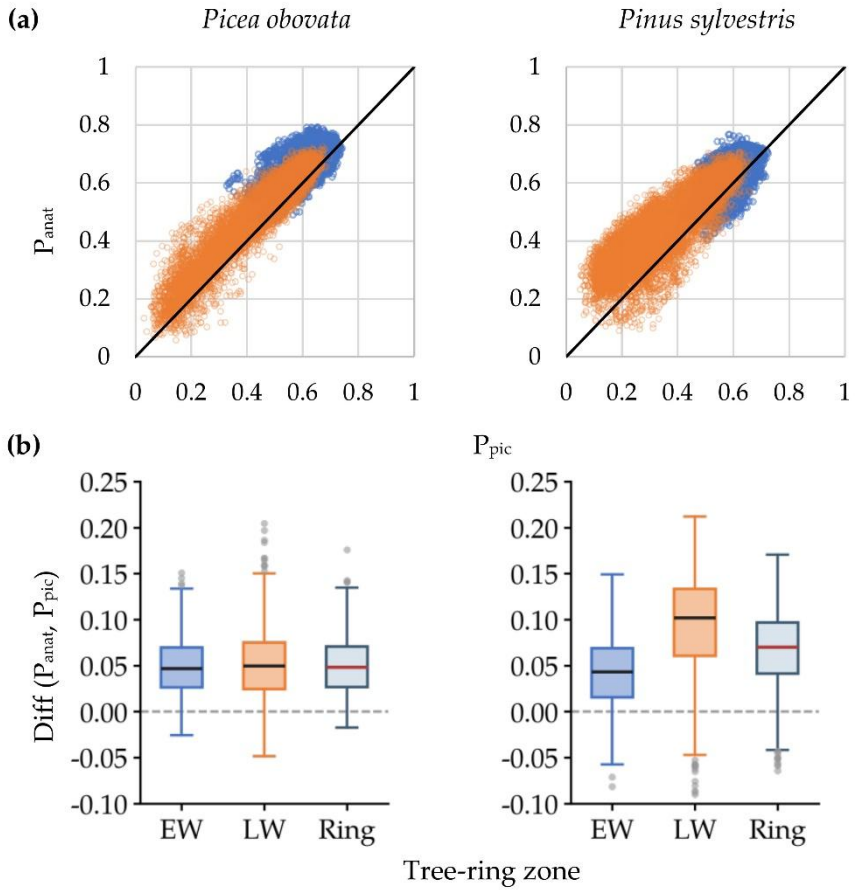


Figure 4. Comparison of the P_{pic} and P_{anat} porosity profiles for all measured tree rings of spruce (*Picea obovata*) and pine (*Pinus sylvestris*) pooled across all cell number groups: (**a**) scatter plots with the earlywood (EW, blue) and latewood (LW, orange) zones highlighted in color; the diagonal represents the 1:1 ratio of porosity values; (**b**) the distribution of the difference $P_{anat} - P_{pic}$ for spruce and pine, separately for earlywood (EW), latewood (LW) and total ring 25th and 75th percentiles (box), median (horizontal line), extreme values within 1.5 interquartile ranges (whiskers), and outliers (points beyond the whiskers).

The sensitivity of the results to the assumed tangential cell diameter was assessed by recalculating Panat for Dt values from 20 to 40 μm in 5-μm increments (Table 3; Figure 5). The agreement between the obtained P_{anat} and P_{pic} (R^2) hardly changed and varied from 0.86 to 0.90 in spruce and from 0.79 to 0.86 in pine, as did the regression slope a (it changed by no more than 0.02). The absolute difference between P_{anat} and P_{pic} changed by 0.02–0.06 with each 5-μm shift in D_t. Starting from D_t = 30 μm, P_{anat} exceeded Ppic in all zones of the tree ring. RMSE was lowest at D_t = 25 μm in both species. The patterns between species and between ring zones, however, did not depend on D_t: in spruce the difference was practically the same in earlywood and latewood (the zone medians differed by no more than 0.01), whereas in pine it was 0.05–0.06 higher in latewood than in earlywood, and the latewood slope in pine (0.73–0.76) remained lower than in spruce (0.83–0.92) at any D_t. We believe that actual measurement of the mean tangential cell diameter for each particular ring (even simplified, e.g., by measuring width of the wide band of radial cell files and dividing it by their number) can improve accuracy of calculation for P_{anat}.

Table 3. Sensitivity of the relationship between P_{anat} and P_{pic} to the assumed tangential tracheid diameter D_t. The regression parameters and error metrics are given for the total ring, and the medians of the difference $P_{anat} - P_{pic}$ for the total ring, earlywood (EW) and latewood (LW); all tree rings of each species are pooled. The rows for D_t = 30 μm (bold) correspond to the "All" rows of Table 2. Other notation as in Table 2.

Species	D_t, μm	Total Ring					Median $P_{anat} - P_{pic}$		
		R^2	*a*	*b*	*MAPE*, %	*RMSE*	Total Ring	EW	LW
Picea obovata	20	0.86	0.89	0.03	10.77	0.06	−0.03	−0.03	−0.03
	25	0.88	0.89	0.08	9.87	0.05	0.02	0.02	0.02
	30	0.89	0.90	0.11	13.70	0.07	0.05	0.05	0.05
	35	0.89	0.90	0.13	18.00	0.09	0.07	0.07	0.08
	40	0.90	0.91	0.14	21.54	0.10	0.09	0.09	0.10
Pinus sylvestris	20	0.79	0.78	0.07	16.75	0.08	−0.04	−0.06	−0.01
	25	0.82	0.77	0.13	17.05	0.07	0.02	0.00	0.05
	30	0.84	0.77	0.17	22.39	0.09	0.06	0.04	0.09
	35	0.85	0.76	0.20	28.15	0.11	0.08	0.06	0.12
	40	0.86	0.76	0.23	33.00	0.13	0.10	0.08	0.14

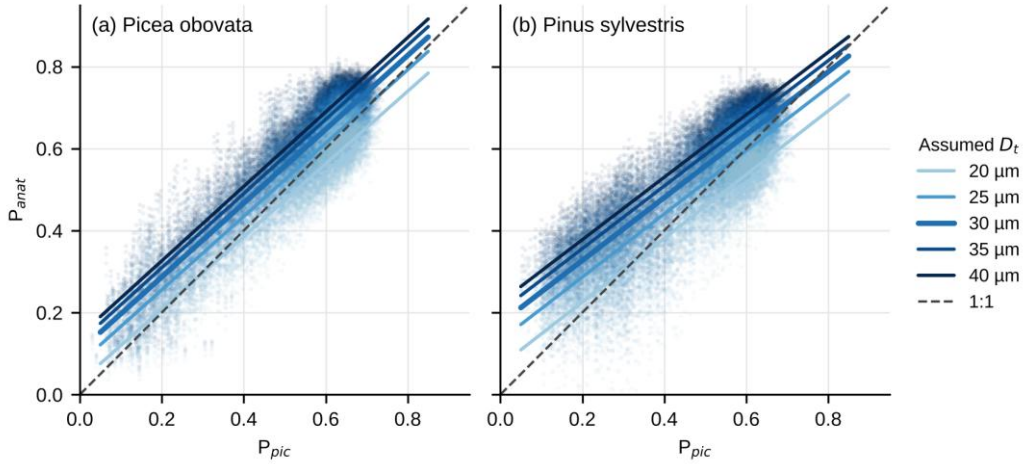


Figure 5. Dependence of the relationship between P_{pic} and P_{anat} on the assumed tangential cell diameter D_t (20–40 μm) for (**a**) spruce (*Picea obovata*) and (**b**) pine (*Pinus sylvestris*). Semi-transparent points show a random subsample of profile points of each species (the same points for all D_t); lines show linear regressions $P_{anat}(P_{pic})$ calculated from all points; the dashed diagonal line is the 1:1 ratio.

In the main analysis, the boundary between earlywood and latewood was defined by the median P_{pic}, i.e., by one of the two compared estimates. To assess the influence of this choice, we repeated the comparison with other criteria: the median P_{anat}, the anatomical criterion CWT/D ≥ k [49], and the Mork criterion [50] (Table 4). The results obtained with the median P_{anat} and the criterion CWT/D ≥ k were close to those for the median P_{pic}: latewood comprised 43–48% of the points (versus 42–45% for P_{pic}); the coefficient of determination R^2 was 0.71–0.88 in latewood and 0.18–0.35 in earlywood (versus 0.72–0.88 in latewood and 0.29–0.35 in earlywood for P_{pic}). The regression slope in pine latewood (0.66–0.73) remained lower than in spruce (0.87–0.88), and the median difference $P_{anat} - P_{pic}$ was positive in both zones and larger in pine latewood (0.07–0.09) than in spruce latewood (0.05). With the Mork criterion (CWT/D ≥ 1/6), the latewood zone was narrower (17% of points in spruce and 26% in pine), and the agreement in it was weaker (R^2 = 0.68 for spruce and 0.23 for pine), whereas in earlywood R^2 was higher (0.62 and 0.54, respectively). The

stricter form of the Mork criterion (2·CWT ≥ L_r) was not used in this study, because with it no latewood was identified in 1 spruce ring and 43 pine rings.

Table 4. Dependence of the relationship between P_{anat} and P_{pic} on the criterion used to delimit earlywood (EW) and latewood (LW). All tree rings of each species are pooled; D_t = 30 μm. k = 0.105 for spruce and 0.110 for pine [49]; Mork criterion according to [50]. L_r, radial lumen diameter. Other notations are as in Table 2.

Boundary Criterion	Species	Zone	Share of Points, %	R^2	*a*	*b*	*MAPE*, %	*RMSE*	Median $P_{anat} - P_{pic}$
Median P_{pic} in the ring (main analysis)	*Picea obovata*	EW	58	0.35	0.54	0.34	9.00	0.07	0.05
		LW	42	0.88	0.89	0.10	20.20	0.08	0.05
	Pinus sylvestris	EW	55	0.29	0.57	0.30	8.23	0.06	0.04
		LW	45	0.72	0.75	0.18	39.49	0.11	0.09
Median P_{anat} in the ring	*Picea obovata*	EW	57	0.33	0.51	0.36	9.13	0.07	0.05
		LW	43	0.88	0.88	0.11	19.68	0.08	0.05
	Pinus sylvestris	EW	56	0.35	0.58	0.29	8.58	0.06	0.04
		LW	44	0.71	0.73	0.18	39.95	0.11	0.09
CWT/*D* ≥ k_a	*Picea obovata*	EW	57	0.18	0.39	0.43	8.65	0.06	0.05
		LW	43	0.85	0.87	0.11	20.46	0.08	0.05
	Pinus sylvestris	EW	52	0.20	0.36	0.43	9.21	0.06	0.05
		LW	48	0.72	0.66	0.20	36.41	0.11	0.07
Mork criterion, 4·CWT ≥ L_r (CWT/*D* ≥ 1/6)	*Picea obovata*	EW	83	0.62	0.72	0.22	9.68	0.07	0.05
		LW	17	0.68	0.81	0.11	33.52	0.09	0.06
	Pinus sylvestris	EW	74	0.54	0.62	0.26	10.73	0.07	0.04
		LW	26	0.23	0.43	0.24	55.51	0.13	0.11

The mean profile of the species, i.e., the dependence of porosity on the relative position within the tree ring, explained 76% of the variance of P_{pic} in spruce and 80% in pine. After subtracting the mean profile from both estimates, R^2 decreased from 0.89 to 0.57 in spruce and from 0.84 to 0.42 in pine (Figure 6c,f); the agreement of the residuals was still higher in latewood (R^2 = 0.70 and 0.48) than in earlywood (0.26 in both species). The mean standard deviation of the pair of estimates (P_{pic}, P_{anat}) was 0.04 in spruce and 0.05 in pine, i.e., 63% and 75% of the standard deviation of P_{pic} among rings at the same position; in earlywood it was comparable to the variability among rings, whereas in latewood it was considerably lower (Figure 6b,e).

The testing of conventional assumption that CWT is equal in both directions demonstrated that in latewood, it is likely incorrect. When P_{anat} was recalculated for latewood using Equation (1) (Figure 7), the systematic excess of P_{anat} over P_{pic} in latewood decreased as k_w increased: the median difference decreased from +0.053 (at k_w = 1.0) to 0.001 (at k_w = 1.3) for spruce, and from +0.090 (at k_w = 1.0) to +0.029 (at k_w = 1.3) and −0.012 (at k_w = 1.5) for pine. The slope of the regression line for the whole tree ring approached 1 (1.01 at k_w = 1.3 for spruce and 1.01 at k_w = 1.5 for pine). R^2 for the whole ring changed only slightly (0.85–0.89 for spruce and 0.84–0.85 for pine), while RMSE reached its minimum at $k_w \approx 1.3$ for spruce (0.062) and at $k_w \approx 1.4$ for pine (0.070). The slope of the regression line for latewood remained below 1 at all values of k_w (0.83–0.89 for spruce and 0.73–0.75 for pine).

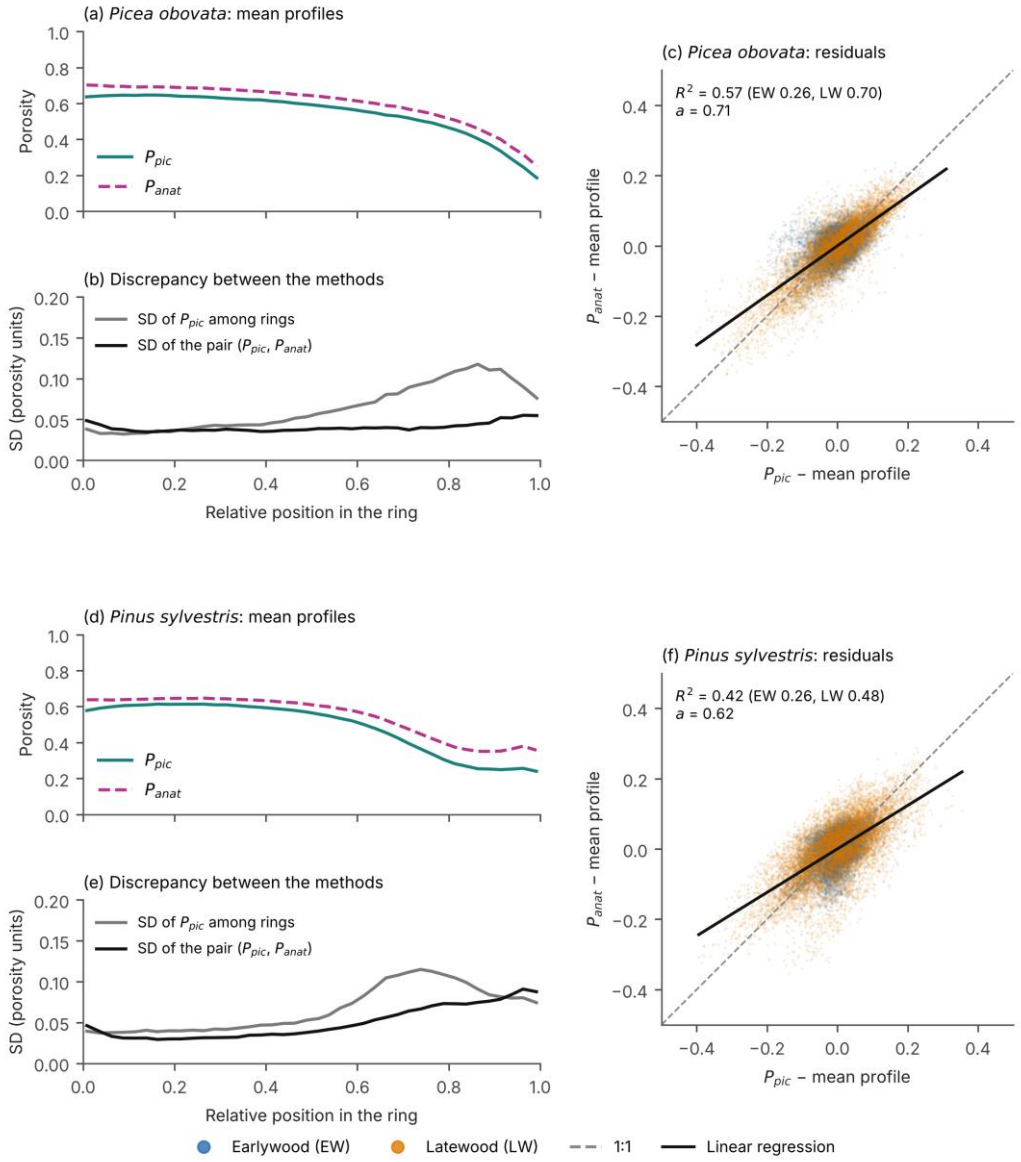


Figure 6. Agreement between P_{anat} and P_{pic} after removal of the common course of porosity across the ring for (**a**–**c**) spruce (*Picea obovata*) and (**d**–**f**) pine (*Pinus sylvestris*). (**a**,**d**) Mean profiles of P_{pic} and P_{anat} as functions of the relative position in the ring (mean values in 40 equal intervals); they were subtracted from the corresponding estimates. (**b**,**e**) Standard deviation (SD) of the pair of estimates (P_{pic}, P_{anat}) of each cell, averaged over the intervals of relative position, compared with the SD of P_{pic} among rings in the same interval. (**c**,**f**) Relationship between the residuals; earlywood (EW) in blue, latewood (LW) in orange; the dashed line is 1:1, the solid line is the linear regression. The R^2 values are given for all points, EW and LW; *a*, regression slope. All tree rings of each species are pooled; D_t = 30 μm.

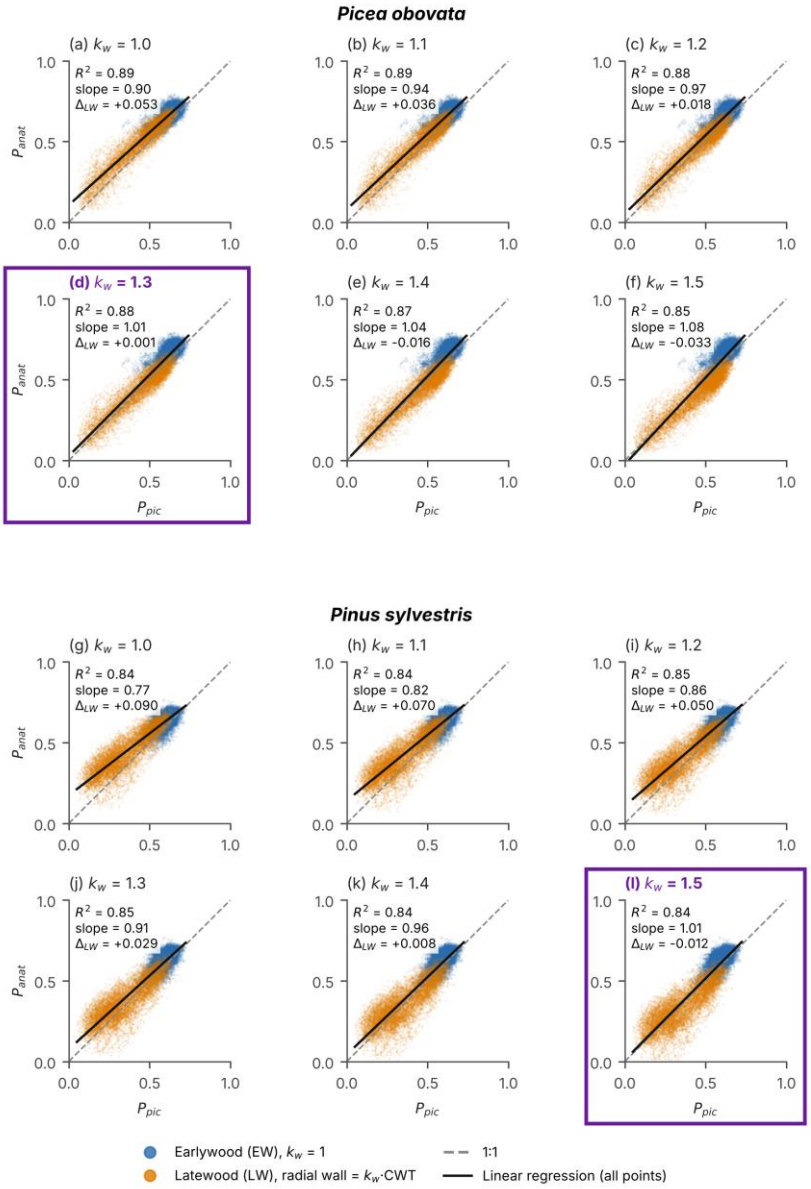


Figure 7. Relationship between P_{anat} and P_{pic} at different ratios (k_w = CWT_t/CWT) of the cell wall thickness in the tangential direction to that in the radial direction in latewood (k_w = 1.0–1.5; k_w = 1 in earlywood) for (**a**–**f**) spruce (*Picea obovata*) and (**g**–**l**) pine (*Pinus sylvestris*). Earlywood (EW) in blue, latewood (LW) in orange; the dashed line is 1:1, the solid line is the linear regression for all points. R^2, coefficient of determination; slope, slope of the regression; Δ_{LW}, median difference $P_{anat} - P_{pic}$ in latewood. The frames mark the k_w at which the slope is closest to 1 (k_w = 1.3 in spruce, k_w = 1.5 in pine). All tree rings of each species are pooled; D_t = 30 µm.

4. Discussion

The xylem of spruce, in particular of *Picea obovata* and the closely related boreal Eurasian species *Picea abies* [51,52], is undoubtedly a classical object among conifers, especially its three-dimensional structure [53–55]. Scots pine wood anatomy has been reviewed in detail [19], while the hydraulic architecture of Pinaceae has been considered more broadly [36]. Studies of Scots pine have examined intra-annual cellular characteristics and their relation to density [56], dendroclimatic signals in anatomical traits [57], hydraulic adjustment [58], wood-density variation [59], and embolism spread [60]. This determines the interest in the methodology for estimating quantitative structural parameters, including porosity, for the tree rings of these species.

The presented results of the comparison of conifer wood porosity estimates obtained by the tracheidogram method and by PiC densitometry clearly show a strong linear relationship between these characteristics. The generality and stability of the observed relationships for tree rings over a wide range of widths indicate the robustness of the relationship at the intraspecific level. We therefore consider that both measurement methods are potentially applicable to the dendroclimatic analysis of porosity profiles or their individual statistical parameters (e.g., mean or maximum porosity in the ring), both for the direct problem (features of porosity variation in individual growth years depending on the dynamics of climatic factors) and for the inverse problem, namely the reconstruction of seasonal conditions from tree-ring porosity profiles as a whole or from their individual characteristics. However, the comparison of the two methods provides interesting additional information. Let us consider the possible causes of the discrepancies between the measurements obtained by the two methods. The most likely explanation for the stable excess of anatomical porosity over PiC densitometric porosity is that anatomical measurements are based on tracheid files visually selected from microphotographs for their regular shape and large tangential diameters. In pixel-contrast densitometry, all cells within a given band of the tree ring are measured. We believe that the main difference is determined by the three-dimensional arrangement of tracheids relative to each other [61,62] and to the plane of the cross-section. In the tracheidogram method, visually selecting a tracheid file for measurement makes it likely that the section plane passes through the central parts of the tracheids. Tracheids are spindle-shaped, and their cross-sectional dimensions are greatest in the middle and decrease towards the tips [63,64]. Published measurements place the mean tracheid length of typical *Pinus sylvestris* at approximately 3.37 mm and document variation in tracheid length with cambial age in *Picea obovata* [65,66]. Thus, the selected files may have larger tangential dimensions than files intersected closer to the tracheid tips. As the stem circumference increases, cambial initials sometimes divide anticlinally, producing new initials that contribute to additional tracheid files [67]. Anticlinal divisions can also occur in cells on the xylem side of the initials; in that case, the increase in the number of files is temporary and confined to the xylem [68]. Pixel-contrast densitometry includes these files in the porosity calculation. If their tracheids have smaller lumina relative to their cell-wall thickness, they may lower the measured porosity. Depending on their relative abundance, this could contribute to differences of 0.1–0.15 or more between the porosity estimates, as illustrated by the plots of P_{anat} versus P_{pic} for the tree rings of both species. It should also be taken into account that ray parenchyma and resin ducts can be included in wood porosity during PiC analysis. In this study, resin ducts were removed from the profile at the analysis stage by filtering lumen runs longer than 150 pixels (~64 μm; Section 2.3), so that smaller ducts could remain in the calculation. At the same time, rays can considerably reduce wood porosity in some areas. The tangential cell diameter assumed in the anatomical model is another factor affecting the absolute difference between the estimates. The strong relationship between the estimates and the considerable difference between them in pine latewood show little relation to D_t (Table 3, Figure 5). The excess of P_{anat} over P_{pic} may also be explained by P_{pic} including smaller tracheids than those selected for the tracheidogram, so that the effective mean tangential diameter of all cells in the scanned area is smaller than that of the measured files. However, the influence of other factors cannot be excluded. Thus, the systematic differences between P_{pic} and P_{anat} can be interpreted as a consequence of the different objects being measured, which is also a limitation of this study.

Thus, the stable excess of P_{anat} over P_{pic} should be interpreted not as an error of one of the methods but, at least in part, as a consequence of the different objects being measured: P_{anat} characterizes the selected regular files of large tracheids, and P_{pic} the bulk porosity of the whole scanned tissue. This is an inherent limitation of the comparison: separating the

contribution of the object difference from that of the model simplifications would require measuring P_{pic} within the same radial files as the tracheidogram, which is a task for further work.

An important finding is the increase in the difference between the porosity estimates in latewood, evidently manifested in the low slope of the linear relationship between them. This phenomenon is stable for rings of different width but is clearly species-specific, being more pronounced in pine. We assume that this is related to the assumption used in our model of the cell cross-section that the cell wall thickness is by default equal in all directions, which is not obviously and universally true. Indeed, some studies take into account the non-uniformity of cell wall thickness; for example, in modeling Scots pine tracheids [56], the thicknesses of the radial and tangential cell walls in latewood were treated as separate variables. Cuny et al. [69] reported that their radial wall thickness was approximately 1.3 times greater than their tangential wall thickness in latewood. Under the measurement-direction terminology used in this study, this corresponds to a tangential wall thickness approximately 1.3 times greater than a radial wall thickness (Figure 1). Obviously, intermediate values may occur in the transition from earlywood to latewood. Such discrepancy is probably due to local wall thickenings near the cell corners, which almost overlap in the short radial walls of the flattened thick-walled cells of typical latewood (cf. models with and without wall thickening at the corners in [33]). Another study reported the distributions of radial and tangential tracheid wall thickness in the earlywood and latewood of *Pinus massoniana* and *Cunninghamia lanceolata*, demonstrating their distinct species-specificity [70], which is also consistent with the species-specific bias of anatomical latewood porosity in our study. In addition, in the studied plantation, pine shows consistently higher cell wall thickness of latewood tracheids than spruce [39], which probably contributes to the anisotropy of this parameter and, as a result, to the larger difference between the porosity estimates for latewood cells. This effect was not tested directly here because rings were grouped by cell number rather than by site.

In this study, we made an attempt at an indirect estimate of this effect (Figure 7) by varying the parameter CWT_t through the multiplication of CWT by the coefficient k_w. The regression slope closest to 1 was found in spruce at $k_w = 1.3$ (which agrees with other published data [69]) and in pine at $k_w = 1.5$, which may indicate a greater thickness of the tangential walls in pine latewood. Since the regression slope for latewood remained below 1 at any constant k_w, it can be assumed that the ratio of wall thicknesses varies both within a single tree ring and among different trees. Consequently, the analysis presented in Figure 7 is a sensitivity test rather than a calibration: the values of k_w were not measured directly and may reflect the influence of other factors that cause the discrepancies. Direct measurements of cell wall thickness in tangential direction in both studied species are needed to confirm this conclusion. It should also be noted that the agreement in latewood depends on how this zone is delimited.

With the Mork criterion, the thick-walled latewood zone was much narrower, and the agreement in it was considerably weaker ($R^2 = 0.68$ in spruce and 0.23 in pine; Table 4). Nevertheless, the high R^2 values in latewood reported here refer to the broader zone delimited by the median porosity or by the threshold $CWT/D \geq k$.

After subtracting the mean porosity profile, the relationship between the methods remained at $R^2 = 0.57$ in spruce and 0.42 in pine (Figure 6c,f). These results suggest that the high R^2 for the whole tree ring largely reflects the fact that both estimates decrease from earlywood to latewood, rather than agreement between the methods at the local scale (Figure 6a,d). Therefore, the high R^2 values for the whole ring (0.79–0.93) should be interpreted with caution. The low agreement between the methods in earlywood is also a limitation of the comparison and is related to the narrow range of porosity values in this zone. The linearity and closeness (R^2 = 0.79–0.93 for whole rings) of the relationship

between the porosity estimates obtained by the two methods suggest that either of them can be used as a time series to describe the course of porosity (intra-seasonal profile or multi-year series), e.g., for solving the direct and inverse problems of dendroclimatic analysis. However, a close relationship between the estimates does not by itself imply equivalent climate sensitivity or reconstruction performance; this requires a separate analysis of the response of both porosity series to climatic variables. On the other hand, when comparing porosity estimates obtained with different methods (e.g., in a spatial meta-analysis of wood quality based on data from several studies), we recommend treating PiC densitometric porosity as the more representative estimate of the bulk cross-sectional porosity, since it integrates all anatomical elements of the scanned area; independent verification of absolute porosity (e.g., by manual segmentation of a subsample of images) is still needed. In the future, we propose to calculate and introduce corrections for the anatomical porosity estimate, which will at least be species-specific and will probably also depend on site conditions, age category and other factors. Given the stable density of the cell wall substance (about 1.5 g/cm^3; [26]), the same considerations also apply to wood density estimates derived from anatomical and PiC densitometric measurements.

5. Conclusions

The obtained results confirm a strong linear relationship between wood porosity P_{pic} and P_{anat} and, consequently, the classical anatomical characteristics used in the quantitative anatomy of conifers. A substantial part of the whole-ring agreement reflects the shared decrease in porosity from earlywood to latewood. After removing the species mean profile, R^2 was 0.57 in spruce and 0.42 in pine. Nevertheless, it is important to note the systematic deviations between anatomical porosity and porosity derived from pixel-contrast densitometry. These deviations appear to be mainly related to the fundamental difference between the methods in the selection of the analyzed area within the tree ring, as a result of which P_{pic} often had lower values than P_{anat}.

Differences in these deviations were also revealed both between species and between rings of different width. In both species, a systematic overestimation of P_{anat} relative to P_{pic} was observed in all tree-ring zones at the assumed tangential cell diameter of 30 μm; the magnitude of this overestimation, but not its pattern between species and ring zones, depends on this assumption (Table 3). In pine, this excess was more pronounced than in spruce. These differences could be related to the assumptions concerning tracheid shape and the dimensions of the tangential cell walls.

Future work should test species- and habitat-specific corrections for anatomical porosity using direct measurements of tracheid dimensions and radial and tangential cell-wall thicknesses. Other interesting directions to study are inclusion of more species (conifers and angiosperms) and evaluation of the suitability of both methods for dendroclimatic applications using climate-response analyses. However, anatomical estimates of porosity (or density) for angiosperm wood are complicated by its less regular cellular structure [71]; thus, equations and assumptions to be used for them are not yet determined.

Author Contributions: Conceptualization, L.V.B. and E.A.V.; methodology, T.A.K., L.V.B. and E.A.V.; software, T.A.K.; validation, L.V.B., D.G.P., V.A.V. and E.A.B.; formal analysis, T.A.K., L.V.B., D.G.P. and V.A.V.; investigation, T.A.K., D.F.Z. and E.A.B.; resources, E.A.B. and E.A.V.; data curation, D.F.Z., N.B.M. and E.A.B.; writing—original draft preparation, T.A.K. and E.A.V.; writing—review and editing, all authors; visualization, T.A.K. and L.V.B.; supervision, E.A.V.; project administration, E.A.B. and E.A.V.; funding acquisition, E.A.B. All authors have read and agreed to the published version of the manuscript.

Funding: This research was funded by the Russian Science Foundation, project No. 26-17-20021.

Data Availability Statement: The source code of the software created for this study is available at https://github.com/Timofey00/OpenPiCDens (accessed on 19 October 2026). The data presented in this study are available from the corresponding author upon reasonable request.

Acknowledgments: During the preparation of this manuscript, the authors used Claude Opus 5.5 (Anthropic) for the purposes of translating the manuscript from Russian into English and formatting the reference list. The authors have reviewed and edited the output and take full responsibility for the content of this publication.

Conflicts of Interest: The authors declare no conflicts of interest.

References

1. von Arx, G.; Carrer, M. ROXAS—A new tool to build centuries-long tracheid-lumen chronologies in conifers. *Dendrochronologia* **2014**, *32*, 290–293. https://doi.org/10.1016/j.dendro.2013.12.001.
2. von Arx, G.; Crivellaro, A.; Prendin, A.L.; Čufar, K.; Carrer, M. Quantitative wood anatomy—Practical guidelines. *Front. Plant Sci.* **2016**, *7*, 781. https://doi.org/10.3389/fpls.2016.00781.
3. Carrer, M.; Castagneri, D.; Prendin, A.L.; Petit, G.; von Arx, G. Retrospective analysis of wood anatomical traits reveals a recent extension in tree cambial activity in two high-elevation conifers. *Front. Plant Sci.* **2017**, *8*, 737. https://doi.org/10.3389/fpls.2017.00737.
4. De Micco, V.; Carrer, M.; Rathgeber, C.B.K.; Camarero, J.J.; Voltas, J.; Cherubini, P.; Battipaglia, G. From xylogenesis to tree rings: Wood traits to investigate tree response to environmental changes. *IAWA J.* **2019**, *40*, 155–182. https://doi.org/10.1163/22941932-40190246.
5. Ziaco, E.; Biondi, F.; Heinrich, I. Wood cellular dendroclimatology: Testing new proxies in Great Basin bristlecone pine. *Front. Plant Sci.* **2016**, *7*, 1602. https://doi.org/10.3389/fpls.2016.01602.
6. Ziaco, E.; Liang, E. New perspectives on sub-seasonal xylem anatomical responses to climatic variability. *Trees* **2019**, *33*, 973–975. https://doi.org/10.1007/s00468-018-1786-9.
7. Cuny, H.E.; Rathgeber, C.B.K.; Frank, D.; Fonti, P.; Fournier, M. Kinetics of tracheid development explain conifer tree-ring structure. *New Phytol.* **2014**, *203*, 1231–1241. https://doi.org/10.1111/nph.12871.
8. Cartenì, F.; Deslauriers, A.; Rossi, S.; Morin, H.; De Micco, V.; Mazzoleni, S.; Giannino, F. The physiological mechanisms behind the earlywood-to-latewood transition: A process-based modeling approach. *Front. Plant Sci.* **2018**, *9*, 1053. https://doi.org/10.3389/fpls.2018.01053.
9. Sorce, C.; Giovannelli, A.; Sebastiani, L.; Anfodillo, T. Hormonal signals involved in the regulation of cambial activity, xylogenesis and vessel patterning in trees. *Plant Cell Rep.* **2013**, *32*, 885–898. https://doi.org/10.1007/s00299-013-1431-4.
10. Buttò, V.; Deslauriers, A.; Rossi, S.; Rozenberg, P.; Shishov, V.; Morin, H. The role of plant hormones in tree-ring formation. *Trees* **2020**, *34*, 315–335. https://doi.org/10.1007/s00468-019-01940-4.
11. Nguyen, T.T.T.; Bae, E.-K.; Tran, T.N.A.; Lee, H.; Ko, J.-H. Exploring the seasonal dynamics and molecular mechanism of wood formation in gymnosperm trees. *Int. J. Mol. Sci.* **2023**, *24*, 8624. https://doi.org/10.3390/ijms24108624.
12. Silvestro, R.; Deslauriers, A.; Prislan, P.; Rademacher, T.; Rezaie, N.; Richardson, A.D.; Vitasse, Y.; Rossi, S. From roots to leaves: Tree growth phenology in forest ecosystems. *Curr. For. Rep.* **2025**, *11*, 12. https://doi.org/10.1007/s40725-025-00245-9.
13. Seo, J.-W.; Eckstein, D.; Jalkanen, R.; Rickebusch, S.; Schmitt, U. Estimating the onset of cambial activity of Scots pine in northern Finland by means of the heat-sum approach. *Tree Physiol.* **2008**, *28*, 105–112. https://doi.org/10.1093/treephys/28.1.105.
14. Rathgeber, C.B.K.; Cuny, H.E.; Fonti, P. Biological basis of tree-ring formation: A crash course. *Front. Plant Sci.* **2016**, *7*, 734. https://doi.org/10.3389/fpls.2016.00734.
15. Castagneri, D.; Fonti, P.; von Arx, G.; Carrer, M. How does climate influence xylem morphogenesis over the growing season? Insights from long-term intra-ring anatomy in *Picea abies*. *Ann. Bot.* **2017**, *119*, 1011–1020. https://doi.org/10.1093/aob/mcw274.
16. Cabon, A.; Peters, R.L.; Fonti, P.; Martínez-Vilalta, J.; De Cáceres, M. Temperature and water potential co-limit stem cambial activity along a steep elevational gradient. *New Phytol.* **2020**, *226*, 1325–1340. https://doi.org/10.1111/nph.16456.
17. Eckes-Shephard, A.H.; Ljungqvist, F.C.; Drew, D.M.; Rathgeber, C.B.K.; Friend, A.D. Wood formation modeling—A research review and future perspectives. *Front. Plant Sci.* **2022**, *13*, 837648. https://doi.org/10.3389/fpls.2022.837648.
18. Chavchavadze, E.S. *Wood of Conifers: Morphological Features and Diagnostic Significance*; Nauka: Leningrad, Russia, 1979; 192p. (In Russian)

19. Schultze-Dewitz, G.; Koch, G. The anatomy of wood and bark of Scots pine. A review of literature. *Feddes Repert.* **2008**, *119*, 655–668. https://doi.org/10.1002/fedr.200811183.
20. García Esteban, L.; de Palacios de Palacios, P.; Guindeo Casasús, A.; García Fernández, F. Characterisation of the xylem of 352 conifers. *For. Syst.* **2004**, *13*, 452–478. https://doi.org/10.5424/srf/2004133-00846.
21. Silkin, P.P.; Kirdyanov, A.V.; Krusic, P.J.; Ekimov, M.V.; Barinov, V.V.; Büntgen, U. A new approach to measuring tree-ring density parameters. *J. Sib. Fed. Univ. Biol.* **2022**, *15*, 441–455.
22. Khudykh, T.A.; Belokopytova, L.V.; Kholdaenko, Y.A.; Karmanovskaya, N.V.; Portnyagin, D.G.; Babushkina, E.A.; Vaganov, E.A. Tree-ring width and wood porosity of *Pinus sylvestris* L. and *Populus tremula* L. show different climate responses in southern Siberia. *Dendrochronologia* **2026**, *96*, 126502. https://doi.org/10.1016/j.dendro.2026.126502.
23. Vaganov, E.A. The tracheidogram method in tree-ring analysis and its application. In *Methods of Dendrochronology: Applications in the Environmental Sciences*; Cook, E.R., Kairiukstis, L.A., Eds.; Kluwer Academic Publishers: Dordrecht, The Netherlands, 1990; pp. 63–76.
24. Silkin, P.P. *Methods of Multiparameter Analysis of Conifer Tree-Ring Structure*; Siberian Federal University: Krasnoyarsk, Russia, 2010; 335p. (In Russian)
25. Seo, J.-W.; Smiljanić, M.; Wilmking, M. Optimizing cell-anatomical chronologies of Scots pine by stepwise increasing the number of radial tracheid rows included—Case study based on three Scandinavian sites. *Dendrochronologia* **2014**, *32*, 205–209. https://doi.org/10.1016/j.dendro.2014.02.002.
26. Zauer, M.; Pfriem, A.; Wagenführ, A. Toward improved understanding of the cell-wall density and porosity of wood determined by gas pycnometry. *Wood Sci. Technol.* **2013**, *47*, 1197–1211. https://doi.org/10.1007/s00226-013-0568-1.
27. Babushkina, E.A.; Zhirnova, D.F.; Belokopytova, L.V.; Vaganov, E.A. Warming induced changes in wood matter accumulation in tracheid walls of spruce. *J. Mt. Sci.* **2020**, *17*, 16–30. https://doi.org/10.1007/s11629-019-5516-6.
28. Rathgeber, C.B.K.; Decoux, V.; Leban, J.-M. Linking intra-tree-ring wood density variations and tracheid anatomical characteristics in Douglas fir (*Pseudotsuga menziesii* (Mirb.) Franco). *Ann. For. Sci.* **2006**, *63*, 699–706. https://doi.org/10.1051/forest:2006050.
29. Rathgeber, C.B.K. Conifer tree-ring density inter-annual variability—Anatomical, physiological and environmental determinants. *New Phytol.* **2017**, *216*, 621–625. https://doi.org/10.1111/nph.14763.
30. Wilkinson, S.; Ogée, J.; Domec, J.-C.; Rayment, M.; Wingate, L. Biophysical modelling of intra-ring variations in tracheid features and wood density of *Pinus pinaster* trees exposed to seasonal droughts. *Tree Physiol.* **2015**, *35*, 305–318. https://doi.org/10.1093/treephys/tpv010.
31. Kretschmann, D.E. Mechanical properties of wood. In *Wood Handbook—Wood as an Engineering Material*; General Technical Report FPL-GTR-190; Forest Products Laboratory: Madison, WI, USA, 2010; pp. 5-1–5-46.
32. Hacke, U.G.; Sperry, J.S. Functional and ecological xylem anatomy. *Perspect. Plant Ecol. Evol. Syst.* **2001**, *4*, 97–115.
33. Watanabe, U.; Norimoto, M.; Morooka, T. Cell wall thickness and tangential Young's modulus in coniferous early wood. *J. Wood Sci.* **2000**, *46*, 109–114. https://doi.org/10.1007/BF00777356.
34. Qu, W.; Yang, C.; Zhang, J.; Ma, Y.; Tian, X.; Zhao, S.; Yu, W. Hydraulic function analysis of conifer xylem based on a model incorporating tracheids, bordered pits, and cross-field pits. *Forests* **2022**, *13*, 171. https://doi.org/10.3390/f13020171.
35. Lundqvist, S.-O.; Holmqvist, C.; Rosner, S. Towards efficient models for hydraulic conductivity in conifer wood. Part 2: Estimation of variation in hydraulic conductivity within and between annual rings from anatomical data. *Holzforschung* **2025**, *79*, 46–63. https://doi.org/10.1515/hf-2024-0060.
36. Martínez-Vilalta, J.; Sala, A.; Piñol, J. The hydraulic architecture of Pinaceae—A review. *Plant Ecol.* **2004**, *171*, 3–13. https://doi.org/10.1023/B:VEGE.0000029378.87169.b1.
37. Hacke, U.G.; Lachenbruch, B.; Pittermann, J.; Mayr, S.; Domec, J.-C.; Schulte, P.J. The hydraulic architecture of conifers. In *Functional and Ecological Xylem Anatomy*; Hacke, U., Ed.; Springer: Cham, Switzerland, 2015; pp. 39–75. https://doi.org/10.1007/978-3-319-15783-2_2.
38. Wang, L.; Payette, S.; Bégin, Y. Relationships between anatomical and densitometric characteristics of black spruce and summer temperature at tree line in northern Quebec. *Can. J. For. Res.* **2002**, *32*, 477–486. https://doi.org/10.1139/x01-208.
39. Babushkina, E.A.; Kholdaenko, Y.A.; Belokopytova, L.V.; Zhirnova, D.F.; Mapitov, N.B.; Kostyakova, T.V.; Krutovsky, K.V.; Vaganov, E.A. The influence of planting density and climatic variables on the wood structure of Siberian spruce and Scots pine. *Forests* **2025**, *16*, 1622. https://doi.org/10.3390/f16111622.
40. Buzykin, A.I.; Pshenichnikova, L.S.; Sukhovolsky, V.G. *Density and Productivity of Tree Stands*; Nauka: Novosibirsk, Russia, 2002; 151p. (In Russian)

41. Kholdaenko, Y.A.; Belokopytova, L.V.; Zhirnova, D.F.; Upadhyay, K.K.; Tripathi, S.K.; Koshurnikova, N.N.; Sobachkin, R.S.; Babushkina, E.A.; Vaganov, E.A. Stand density effects on tree growth and climatic response in *Picea obovata* Ledeb. plantations. *For. Ecol. Manag.* **2022**, *519*, 120349. https://doi.org/10.1016/j.foreco.2022.120349.
42. Havimo, M.; Rikala, J.; Sirviö, J.; Sipi, M. Tracheid cross-sectional dimensions in Scots pine (*Pinus sylvestris*): Distributions and comparison with Norway spruce (*Picea abies*). *Silva Fenn.* **2009**, *43*, 681–688. https://doi.org/10.14214/sf.188.
43. Havimo, M.; Rikala, J.; Sirviö, J.; Sipi, M. Distributions of tracheid cross-sectional dimensions in different parts of Norway spruce stems. *Silva Fenn.* **2008**, *42*, 89–99. https://doi.org/10.14214/sf.266.
44. Sviderskaya, I.V.; Soukhovolsky, V.G.; Radosteva, E.Y.; Kirdyanov, A.V. Model estimation of optimal ratio between cell wall thickness and lumen size for tracheids of conifers in temperate zone. *J. Sib. Fed. Univ. Biol.* **2011**, *4*, 183–196. (In Russian)
45. García-Hidalgo, M.; García-Pedrero, Á.; Rozas, V.; Sangüesa-Barreda, G.; García-Cervigón, A.I.; Resente, G.; Wilmking, M.; Olano, J.M. Tree ring segmentation using UNEt TRansformer neural network on stained microsections for quantitative wood anatomy. *Front. Plant Sci.* **2024**, *14*, 1327163. https://doi.org/10.3389/fpls.2023.1327163.
46. Yakubovskiy, P. Segmentation Models Pytorch. GitHub Repository. 2020. Available online: https://github.com/qubvel/segmentation_models.pytorch (accessed on 3 August 2026).
47. Kim, S.; Kim, H. A new metric of absolute percentage error for intermittent demand forecasts. *Int. J. Forecast.* **2016**, *32*, 669–679. https://doi.org/10.1016/j.ijforecast.2015.12.003.
48. Hodson, T.O. Root-mean-square error (RMSE) or mean absolute error (MAE): When to use them or not. *Geosci. Model Dev.* **2022**, *15*, 5481–5487. https://doi.org/10.5194/gmd-15-5481-2022.
49. Belokopytova, L.V.; Zhirnova, D.F.; Yang, B.; Babushkina, E.A.; Vaganov, E.A. Modeling of the statistical distribution of tracheids in conifer rings: Finding universal criterion for earlywood–latewood distinction. *Plants* **2023**, *12*, 3454. https://doi.org/10.3390/plants12193454.
50. Denne, M.P. Definition of latewood according to Mork (1928). *IAWA J.* **1989**, *10*, 59–62. https://doi.org/10.1163/22941932-90001112.
51. Krutovskii, K.V.; Bergmann, F. Introgressive hybridization and phylogenetic relationships between Norway, *Picea abies* (L.) Karst., and Siberian, *P. obovata* Ledeb., spruce species studied by isozyme loci. *Heredity* **1995**, *74*, 464–480. https://doi.org/10.1038/hdy.1995.67.
52. Cole, T.C.H. Phylogeny of SPRUCES (Genus Picea). 2024. Available online: https://www.researchgate.net/publication/379248833_Phylogeny_of_SPRUCES_PiceaPP (accessed on 13 October 2026).
53. Lotova, L.I. *Morphology and Anatomy of Higher Plants*, 5th ed.; URSS: Moscow, Russia, 2013; 508p. (In Russian)
54. Schweingruber, F.H. *Anatomy of European Woods*; Haupt: Bern, Switzerland, 1990; 806p.
55. Schweingruber, F.H. *Trees and Wood in Dendrochronology*; Springer: Berlin/Heidelberg, Germany, 1993; 386p. https://doi.org/10.1007/978-3-642-77157-6.
56. Wimmer, R. Intra-annual cellular characteristics and their implications for modeling softwood density. *Wood Fiber Sci.* **1995**, *27*, 413–420.
57. Björklund, J.; Seftigen, K.; Fonti, P.; Nievergelt, D.; von Arx, G. Dendroclimatic potential of dendroanatomy in temperature-sensitive *Pinus sylvestris*. *Dendrochronologia* **2020**, *60*, 125673. https://doi.org/10.1016/j.dendro.2020.125673.
58. Martínez-Vilalta, J.; Cochard, H.; Mencuccini, M.; Sterck, F.; Herrero, A.; Korhonen, J.F.J.; Llorens, P.; Nikinmaa, E.; Nolè, A.; Poyatos, R.; et al. Hydraulic adjustment of Scots pine across Europe. *New Phytol.* **2009**, *184*, 353–364. https://doi.org/10.1111/j.1469-8137.2009.02954.x.
59. Auty, D.; Achim, A.; Macdonald, E.; Cameron, A.D.; Gardiner, B.A. Models for predicting wood density variation in Scots pine. *Forestry* **2014**, *87*, 449–458. https://doi.org/10.1093/forestry/cpu005.
60. Torres-Ruiz, J.M.; Cochard, H.; Mencuccini, M.; Delzon, S.; Badel, E. Direct observation and modelling of embolism spread between xylem conduits: A case study in Scots pine. *Plant Cell Environ.* **2016**, *39*, 2774–2785. https://doi.org/10.1111/pce.12840.
61. Yatsenko-Khmelevsky, A.A. A *Short Course in Plant Anatomy*; Vysshaya Shkola: Moscow, Russia, 1961; 282p. (In Russian)
62. Adey-Johnson, R.; McLean, J.P.; Van den Bulcke, J.; Van Acker, J.; McDonald, P.J. Micro-CT measurements of within-ring variability in longitudinal hydraulic pathways in Norway spruce. *IAWA J.* **2020**, *41*, 12–29. https://doi.org/10.1163/22941932-00002104.
63. Sirviö, J. Variation of cross-sectional properties within single Norway spruce tracheids. *Wood Fiber Sci.* **2001**, *33*, 16–25.
64. Koddenberg, T. A new dimension in wood anatomy education: Exploring softwood and hardwood structures in 3D. *Eur. J. Wood Wood Prod.* **2025**, *83*, 201. https://doi.org/10.1007/s00107-025-02329-6.

65. Yaman, B. Comparative wood anatomy of *Pinus sylvestris* and its var. *compacta* in the West Black Sea region of Turkey. *IAWA J.* **2007**, *28*, 75–82. https://doi.org/10.1163/22941932-90001620.
66. Sarkhad, M.; Ishiguri, F.; Nezu, I.; Tumenjargal, B.; Takahashi, Y.; Baasan, B.; Chultem, G.; Ohshima, J.; Yokota, S. Modeling of radial variations in wood properties and comparison of juvenile and mature wood of four common conifers in Mongolia. *Holzforschung* **2022**, *76*, 14–25. https://doi.org/10.1515/hf-2021-0107.
67. Bannan, M.W. Tracheid size and anticlinal divisions in the cambium of *Pseudotsuga*. *Can. J. Bot.* **1964**, *42*, 603–631. https://doi.org/10.1139/b64-057.
68. Bannan, M.W. Anticlinal divisions and the organization of conifer cambium. *Bot. Gaz.* **1968**, *129*, 107–113. https://doi.org/10.1086/336421.
69. Cuny, H.E.; Fonti, P.; Rathgeber, C.B.K.; von Arx, G.; Peters, R.L.; Frank, D.C. Couplings in cell differentiation kinetics mitigate air temperature influence on conifer wood anatomy. *Plant Cell Environ.* **2019**, *42*, 1222–1232. https://doi.org/10.1111/pce.13464.
70. Meng, Q.; Fu, F.; Wang, J.; He, T.; Jiang, X.; Zhang, Y.; Yin, Y.; Li, N.; Guo, J. Ray Traits of Juvenile Wood and Mature Wood: Pinus massonia and Cunninghamia lanceolata. *Forests* **2021**, *12*, 1277. https://doi.org/10.3390/f12091277.
71. Peters, R.L.; Klesse, S.; Van den Bulcke, J.; Jourdain, L.M.; von Arx, G.; Anadon-Rosell, A.; Krejza, J.; Kahmen, A.; Fonti, M.; Prendin, A.L.; et al. Quantitative vessel mapping on increment cores: A critical comparison of image acquisition methods. *Front. Plant Sci.* **2025**, *16*, 1502237. https://doi.org/10.3389/fpls.2025.1502237.

Disclaimer/Publisher's Note: The statements, opinions and data contained in all publications are solely those of the individual author(s) and contributor(s) and not of MDPI and/or the editor(s). MDPI and/or the editor(s) disclaim responsibility for any injury to people or property resulting from any ideas, methods, instructions or products referred to in the content.